

RESEARCH ARTICLE

10.1002/2016JD025197

Key Points:

- Large HONO emissions observed from biomass burning, with HONO accounting for 2 to 14% of emitted reactive nitrogen
- Direct HONO emissions from power plants measured at night ranged from 0 to 0.4% of emitted NO_x
- Within 15 pptv uncertainty, HONO was indistinguishable from zero outside of recently emitted plumes from known combustion sources

Correspondence to:

J. A. Neuman,
andy.neuman@noaa.gov

Citation:

Neuman, J. A., et al. (2016), HONO emission and production determined from airborne measurements over the Southeast U.S., *J. Geophys. Res. Atmos.*, 121, 9237–9250, doi:10.1002/2016JD025197.

Received 6 APR 2016

Accepted 21 JUL 2016

Accepted article online 26 JUL 2016

Published online 13 AUG 2016

HONO emission and production determined from airborne measurements over the Southeast U.S.

J. A. Neuman^{1,2}, M. Trainer², S. S. Brown², K.-E. Min^{1,2,3}, J. B. Nowak^{1,2,4}, D. D. Parrish^{1,2}, J. Peischl^{1,2}, I. B. Pollack^{1,2,5}, J. M. Roberts², T. B. Ryerson², and P. R. Veres^{1,2}

¹Cooperative Institute for Research in Environmental Sciences, University of Colorado Boulder, Boulder, Colorado, USA, ²Chemical Sciences Division, NOAA Earth System Research Laboratory, Boulder, Colorado, USA, ³Now at School of Environmental Science and Engineering, Gwangju Institute of Science and Technology, Gwangju, South Korea, ⁴Now at Aerodyne Research, Inc., Billerica, Massachusetts, USA, ⁵Now at Department of Atmospheric Science, Colorado State University, Fort Collins, Colorado, USA

Abstract The sources and distribution of tropospheric nitrous acid (HONO) were examined using airborne measurements over the Southeast U.S. during the Southeast Nexus Experiment in June and July 2013. HONO was measured once per second using a chemical ionization mass spectrometer on the NOAA WP-3D aircraft to assess sources that affect HONO abundance throughout the planetary boundary layer (PBL). The aircraft flew at altitudes between 0.12 and 6.4 km above ground level on 18 research flights that were conducted both day and night, sampling emissions from urban and power plant sources that were transported in the PBL. At night, HONO mixing ratios were greatest in plumes from agricultural burning, where they exceeded 4 ppbv and accounted for 2–14% of the reactive nitrogen emitted by the fires. The HONO to carbon monoxide ratio in these plumes from flaming stage fires ranged from 0.13 to 0.52%. Direct HONO emissions from coal-fired power plants were quantified using measurements at night, when HONO loss by photolysis was absent. These direct emissions were often correlated with total reactive nitrogen with enhancement ratios that ranged from 0 to 0.4%. HONO enhancements in power plant plumes measured during the day were compared with a Lagrangian plume dispersion model, showing that HONO produced solely from the gas phase reaction of OH with NO explained the observations. Outside of recently emitted plumes from known combustion sources, HONO mixing ratios measured several hundred meters above ground level were indistinguishable from zero within the 15 parts per trillion by volume measurement uncertainty. The results reported here do not support the existence of a ubiquitous unknown HONO source that produces significant HONO concentrations in the lower troposphere.

1. Introduction

Photolysis of nitrous acid (HONO) produces OH radicals that are important oxidation agents in atmospheric chemistry. At night, HONO acts as a radical reservoir and affects photochemistry after sunrise by dissociating to form OH and NO. OH from HONO photolysis can promote VOC oxidation, which leads to ozone formation in the presence of NO_x (NO + NO₂). Although atmospheric HONO has been measured for several decades [Perner and Platt, 1979], sources of HONO to the atmosphere remain uncertain [e.g., Stutz et al., 2002; Kleffmann, 2007; Zhou et al., 2011; Li et al., 2014; VandenBoer et al., 2015; Gall et al., 2016]. HONO sources include direct emission from combustion [Kirchstetter et al., 1996; Kurtenbach et al., 2001; Stutz et al., 2002; Wood et al., 2008; Jurkat et al., 2011; Burling et al., 2011] and soils [Oswald et al., 2013], formation by gas phase reaction of OH and NO [Calvert et al., 1994], and production by surface reaction of nitrogen-containing compounds [e.g., Stutz et al., 2004; Stemmler et al., 2006; Kleffmann, 2007; Zhou et al., 2011; VandenBoer et al., 2013; Baergen et al., 2015]. During the day, rapid photolysis (11 min lifetime for solar zenith angle < 20°) [Stockwell and Calvert, 1978] limits HONO mixing ratios. The combination of sources at the surface and rapid photolytic loss in the atmosphere often results in strong daytime HONO vertical gradients [Kleffmann, 2007; Zhang et al., 2009; Wong et al., 2012; Young et al., 2012; VandenBoer et al., 2013]. Many studies have reported such large daytime HONO mixing ratios that they invoked unknown HONO sources to explain the observations [e.g., Kleffmann et al., 2003; Li et al., 2014; Gall et al., 2016]. At night, reduced losses combined with ongoing combustion and production on surfaces allow HONO to accumulate in the atmosphere [Lammel and Cape, 1996; Stutz et al., 2004].

HONO near ground level has been studied in many locations and seasons, but there have been very few investigations that examine HONO distributions throughout the troposphere [Zhang et al., 2009; Li et al., 2014].

Measurements from aircraft flying hundreds of meters above the ground highlight the influence of HONO sources that affect the full depth of the planetary boundary layer (PBL) but cannot probe the near-surface layer where HONO mixing ratios are expected to be at a maximum. In this study, an instrumented aircraft flew in close proximity to urban areas and point sources to directly sample emissions from individual sources and quantify their contribution to atmospheric HONO abundance.

2. Experiment

Instruments aboard the NOAA WP-3D aircraft platform sampled the lower troposphere in June and July 2013 to study air quality and climate as part of the Southeast Nexus Experiment (SENEX, <http://www.esrl.noaa.gov/csd/projects/senex/>), which was under the umbrella of the Southeast Atmosphere Study. Anthropogenic emissions and the resulting secondary product formation were studied by targeting plumes from power plants, urban areas, industrial sources, and regions with extensive oil and natural gas extraction. In situ measurements were obtained on 16 research flights that originated in Smyrna, Tennessee, and 2 transit flights between Smyrna and Tampa, Florida. Flights averaged 6.5 h in duration, and were conducted during both day (14 flights) and night (4 flights). The aircraft usually flew in the PBL at 0.5–0.6 km above ground level (agl), with occasional vertical profiles that typically reached 5 km altitude and with a maximum altitude of 6.4 km. During the daytime flights, the aircraft ordinarily stayed above 0.4 km agl, while the night flights included several descents to 0.12 km agl in order to probe the nocturnal boundary layer. Most daytime flights were conducted from 10 A.M. to 5:30 P.M. central daylight time (CDT). The three nighttime flights analyzed here were conducted from 8 P.M. to 3 A.M. CDT (two flights) and 5:30 P.M. to 11:30 P.M. CDT. Flight locations, sampling strategy, and aircraft payload are further described by *Warneke et al.* [2016]. Since no aircraft measurements were conducted between 3 and 9 A.M. CDT, emissions and photochemistry during morning peak vehicle traffic and the HONO buildup before sunrise [e.g., *Czader et al.*, 2012] are not directly investigated here.

2.1. Trace Gas Detection With a Chemical Ionization Mass Spectrometer

HONO was measured by chemical ionization mass spectrometry (CIMS) using an airborne quadrupole mass spectrometer previously used to measure atmospheric nitric acid (HNO_3) [*Neuman et al.*, 2002] and halogens [*Neuman et al.*, 2010] from the NOAA WP-3D. Air was brought into the instrument through a 70 cm long Teflon line (0.64 cm ID, heated to 40°C). The total inlet flow was approximately 8 standard liters per min (sLpm), of which 1.9 L/min passed through an orifice into a reduced pressure (27 hPa) flow tube where the air was mixed with reagent ions. Reagent ions clustered with gas phase molecules to form unique product ions. These ions then went through an orifice into a chamber at 4×10^{-4} torr, where lenses guided ions toward the detector. The mean free path in this region was greater than 12 cm to reduce collisional dissociation and preserve these ion clusters in the quadrupole mass spectrometer that filtered ions according to their charge to mass ratio.

The reagent ions used during SENEX were negatively charged iodide (I^-) and its water cluster ($\text{I}^- \cdot \text{H}_2\text{O}$), which were made by flowing $1 \text{ cm}^3 \text{ min}^{-1}$ STP of 1010 ppmv methyl iodide in 2 sLpm nitrogen (N_2) through a radioactive ^{210}Po ion source. Detection sensitivity depends on water abundance in the ion-molecule reaction region [*Neuman et al.*, 2010; *Lee et al.*, 2014], because reaction rates with I^- and $\text{I}^- \cdot \text{H}_2\text{O}$ differ. Water was added to the flow tube to control the clustering of water with the I^- reagent ions and to prevent sensitivity fluctuations with changing water concentration in flight. A $10 \text{ cm}^3 \text{ min}^{-1}$ STP flow of N_2 was bubbled through deionized water and added to the flow tube to maintain $\text{I}^- \cdot \text{H}_2\text{O}$ abundance in the drier atmosphere above the boundary layer. The ratio of $\text{I}^- \cdot \text{H}_2\text{O}$ to I^- reagent ion signals averaged 1.7 ± 0.2 over an entire flight and did not depend strongly on ambient humidity. The second water cluster, $\text{I}^- \cdot (\text{H}_2\text{O})_2$, was typically one fourth as abundant as either I^- or $\text{I}^- \cdot \text{H}_2\text{O}$. The product ions also clustered with water (e.g., $\text{I}^- \cdot \text{HONO} \cdot \text{H}_2\text{O}$). For the humidity and analyzer conditions reported here, the unhydrated product ions (e.g., $\text{I}^- \cdot \text{HONO}$) were at least an order of magnitude more abundant than any of their water clusters. A $6 \text{ cm}^3 \text{ min}^{-1}$ STP flow of ammonia was added to the flow tube to reduce signals by suppressing desorption of acidic species from instrument surfaces [*Neuman et al.*, 2002].

Detecting atmospheric gas phase species using I^- clusters, rather than core ions that could originate from fragmentation of several parent ions, reduces the possibility for interferences. I^- is naturally monoisotopic

with a mass of 127 atomic mass units (amu). During the SENEX study, gas phase formic acid (HCOOH, 46 amu), HONO (47 amu), and nitric acid (HNO₃, 63 amu) were measured using the cluster ions at 173 (127 + 46) amu, 174 (127 + 47) amu, and 190 (127 + 63) amu, respectively. The mass spectrometer was tuned to resolve ions separated by 1 amu. Mass peaks had a full width at half maximum of 0.7 amu, and ion signals decreased by over 3 orders of magnitude 1 amu from the center of each mass peak. Each compound was measured once per second by integrating signals at each mass for a fraction of a second in a repeating sequence with a 1 s period. I⁻ and I⁻·H₂O signals at 127 and 145 amu used for diagnostic purposes were measured for 50 ms each, and signals at each of the three ion cluster masses were measured for 200–350 ms each second.

In-flight instrument diagnostics included periodic mass scans from 100 to 250 amu to assess the stability of the mass spectrometer and ion chemistry, as well as in-flight instrument zeros and calibrations. A pneumatically actuated Teflon valve located 4 cm from the inlet tip enabled switching between directly sampling ambient air and diverting the sample flow through a scrubber containing activated charcoal that removed HCOOH, HONO, and HNO₃. Scrubbed ambient air was sampled for 90 s every 0.5 h to quantify the instrument background signal. Interpolating between these instrument background determinations gave a background contribution to the signal at each mass. This background was subtracted from the total signal to derive the signal from ambient air alone. Background variability that was not captured by the periodic background determinations contributed to the measurement uncertainty for each species (discussed below).

Signals were converted to mixing ratios using the instrument response to calibrated gas standards. A continuous 50 cm³ min⁻¹ STP N₂ flow through temperature-controlled ovens containing either HCOOH or HNO₃ permeation tubes was periodically admitted into the inlet for 90 s through a port located 7 cm from the inlet tip. HCOOH or HNO₃ calibrations were performed approximately 10 times every flight. The HCOOH permeation tube emission was determined in the laboratory by catalytic oxidation to CO₂ followed by CO₂ detection [Veres *et al.*, 2010a] before and after the field campaign. The HNO₃ permeation tube output was measured by optical absorption at 185 nm and was monitored continuously on the ground between flights [Neuman *et al.*, 2003]. The HCOOH calibration mixing ratio in the inlet was 3.6 ppbv, and the HNO₃ calibration mixing ratio was 1.1 ppbv. Following the removal of the calibration gases, both HNO₃ and HCOOH signals decayed with an *e*-folding time of approximately 1 s, demonstrating that the instrument had a 1 s time response for these species. Calibrations were performed in both ambient air and in scrubbed ambient air, and detection sensitivity and the reagent ion signals were the same in both. HONO calibration was performed in the laboratory prior to the study, using HONO produced by reacting gas phase HCl with a humidified bed of solid NaNO₂ [Roberts *et al.*, 2010]. Humidifying the flow tube decreased HONO sensitivity and increased HNO₃ and HCOOH sensitivities. This indicates that HONO more favorably clustered with I⁻, while HNO₃ and HCOOH reacted preferentially with I⁻·H₂O.

2.2. Measurement Uncertainties

Atmospheric HONO measurement is susceptible to artifacts introduced by the gas sampling system and detector [e.g., Roberts *et al.*, 2010], and potential interferences must be addressed to guarantee reliable HONO data [Kleffmann and Wiesen, 2008]. Positive interferences can originate in the CIMS if product ions used for HONO detection also originate from reactions with other compounds. The CIMS technique employed here does not use collisional dissociation but rather detects cluster ions. Consequently, these measurements are not compromised by the formation of nitrite ions in the flow tube from other reactions, which can compromise CIMS measurements of HONO [Roberts *et al.*, 2010]. The small contribution to the HONO signal from an isotope of HCOOH is accounted for here. HCOOH isotopes (primarily from ¹³C) contribute 1.1% of the I⁻·HCOOH signal at 173 amu to mass 174 amu used for HONO detection. By quantifying HCOOH, the signal at 174 amu was corrected for the HCOOH contribution before determining HONO mixing ratios. This correction was successful, as demonstrated by the response of the HONO signals during in-flight HCOOH calibrations. The corrected signal at 174 amu corresponding to HONO was unchanged during 3.6 ppbv HCOOH calibration additions.

Positive interferences can also come from NO₂ conversion on humid surfaces to form HONO [Kleffmann and Wiesen, 2008], but the instrument conditions here reduce this interference. The ammonia added to the flow tube to suppress HNO₃ desorption from instrument surfaces [Neuman *et al.*, 2002] also suppresses HONO desorption. Ambient data further indicate that HONO measured here is not formed from conversion of

NO₂ on inlet surfaces, since many plumes were sampled with tens of ppbv NO₂ and no detectable (<15 parts per trillion by volume (pptv)) HONO. Laboratory tests with NO₂ also demonstrated that NO₂ did not interfere with the HONO measurements. The instrument was tested and found to be insensitive to ethanol and NO₂, which could also cause interferences to HCOOH detection if they clustered with I⁻ since they have the same unit mass as HCOOH. Laboratory tests showed no response to the HCOOH and HONO signals from the addition of ethanol and NO₂ at ppmv levels that are much greater than typical ambient mixing ratios encountered in flight. Further, there was no change in the HCOOH signal at 173 amu when the aircraft sampled power plant plumes with tens of ppbv of NO₂.

Negative artifacts may arise if the reaction of NO₂ and water on surfaces in the charcoal scrubber produced and released HONO, which would spuriously increase the measured instrument background. The in-flight background measurements demonstrated that the scrubber did not bias the measurements by releasing HONO. Although there is some variability in the HONO background, the background levels did not vary with NO₂, even during background determinations performed in fire and power plant plumes with tens of ppbv of NO₂. Further, the HONO signal throughout each background determination was constant and without a spike at the background initiation, showing that HONO did not accumulate in the scrubber during half hour periods without flow.

Uncertainties were determined from the calibration response, instrument background variability, and measurement precision. Averaging data for longer periods improves the measurement precision, but it does not reduce inaccuracies caused by instrument background and calibration uncertainties. For HONO, the sensitivity was 1 ion count/s/pptv and the equivalent instrument background was 160 ± 30 pptv. The 1σ measurement precision for 1 s data was 25 pptv, and the accuracy was ± (40% + 30 pptv), where the first term was derived from laboratory calibrations and the second was the in-flight background variability. The sum (in quadrature) of the background uncertainty and imprecision gives a 40 pptv detection limit (1σ) for 1 s data. Averaging the 1 s data for periods greater than the 30 min interval between successive background determinations can improve the detection limit to 15 pptv (section 4.3). For HCOOH and HNO₃, detection sensitivities were typically 1.8 and 2.5 ion counts/s/pptv, respectively. The instrument background for HCOOH was 600 ± 120 pptv, the 1σ precision was 40 pptv for 1 s data, and the accuracy was ± (20% + 120 pptv). The instrument background for HNO₃ was 400 ± 50 pptv, the 1σ precision was 25 pptv, and the accuracy was ± (20% + 50 pptv). The 20% HCOOH and HNO₃ measurement uncertainties were determined by the variability in the instrument response to in-flight calibrations.

Additional measurements were used to analyze and interpret the HONO observations. Most instruments reported data once per second, and the WP-3D flew at 0.1 km s⁻¹. NO, NO₂, and NO_y (= NO + NO₂ + HNO₃ + PAN, ...) mixing ratios were measured using ozone-induced chemiluminescence of NO. NO₂ was measured with 5% uncertainty [Pollack *et al.*, 2011] by first photolyzing atmospheric NO₂ to NO. The sum of gas phase reactive nitrogen species, NO_y, was measured with 10% uncertainty by reducing reactive nitrogen to NO on a gold converter at 300°C. The 1 s measurements of CO were performed with 5% uncertainty and 1 ppbv precision using a vacuum ultraviolet fluorescence instrument [Holloway *et al.*, 2000]. SO₂ was measured once per second with 20% uncertainty using ultraviolet pulsed fluorescence.

3. Results

HONO mixing ratios larger than the detection limit were observed in plumes from several combustion sources. HONO emissions are quantified using nighttime measurements, and photochemical HONO production is examined using daytime measurements.

3.1. Fire Plumes Sampled at Night

HONO emissions from fires were quantified using nighttime measurements, when HONO loss by photolysis was absent. During the SENEX study, the largest HONO mixing ratios were observed after sunset from 8:30 P.M. to 11:30 P.M. CDT on 2 July 2013 in plumes from agricultural fires. These fires were characterized by flaming combustion rather than smoldering, as indicated by CO to CO₂ enhancement ratios that were less than 0.8% and modified combustion efficiencies [Yokelson *et al.*, 2007] that ranged from 0.92 to 0.96. In these plumes, HONO mixing ratios exceeded 4 ppbv and were strongly correlated with other direct fire emissions, including CO and NO_y (Figure 1). The enhancement ratio of HONO to CO (HONO:CO) in the fire plumes was determined

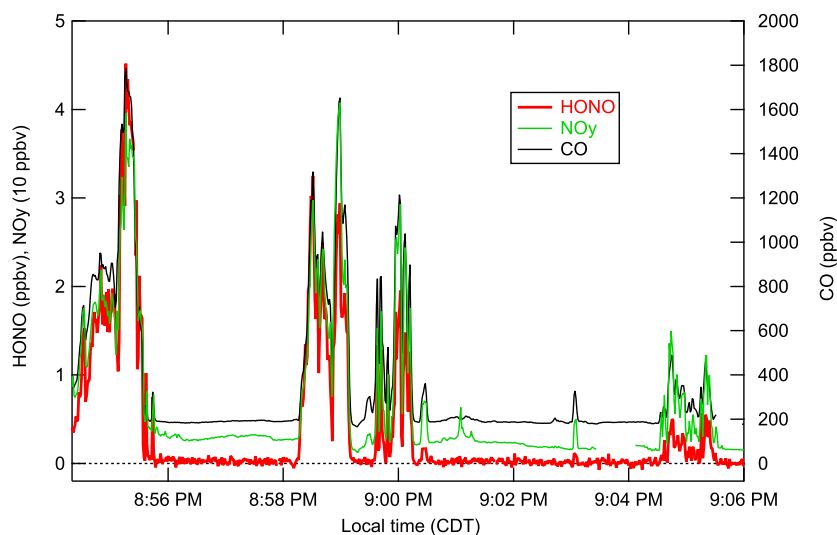


Figure 1. The 1 s measurements of HONO (red), CO (black), and NO_y (green) in agricultural fire plumes sampled at night. The aircraft flew at an altitude between 0.6 and 0.8 km agl over western Tennessee on 3 July 2013. The dashed line is at zero for the left and right axes.

using linear least squares fits of 1 s measurements in individual plumes. In more than 20 individual plume transects on this flight, the HONO:CO varied from 0.13 to 0.52% and averaged $0.24 \pm 0.04\%$, where the uncertainty represents one standard deviation of the mean. As an example, 1 s measurements of HONO and CO in four plumes are shown in Figure 2, where HONO:CO varied from 0.16% (green circles) to 0.27% (red circles). These findings are consistent with laboratory and field studies that sampled fire emissions from Southeastern U.S. and pine fuels, where the flaming stage HONO:CO ranged from approximately 0.2–0.5% [Yokelson *et al.*, 2007; Veres *et al.*, 2010b; Akagi *et al.*, 2011; Burling *et al.*, 2011; Müller *et al.*, 2016].

The enhancement ratio of other fire emissions also varied between plume transects. For example, the enhancement ratio of NO_y to CO in these fire plumes measured at night ranged from 1.5 to 5%. The relationship between HONO and other reactive nitrogen compounds was even more variable than that between HONO and CO. Reactive nitrogen emissions are examined relative to NO_y , since NO_y is conserved with respect to NO_x oxidation on short (hours) time scales. In these plumes, NO_x accounted for over 80% of NO_y . The

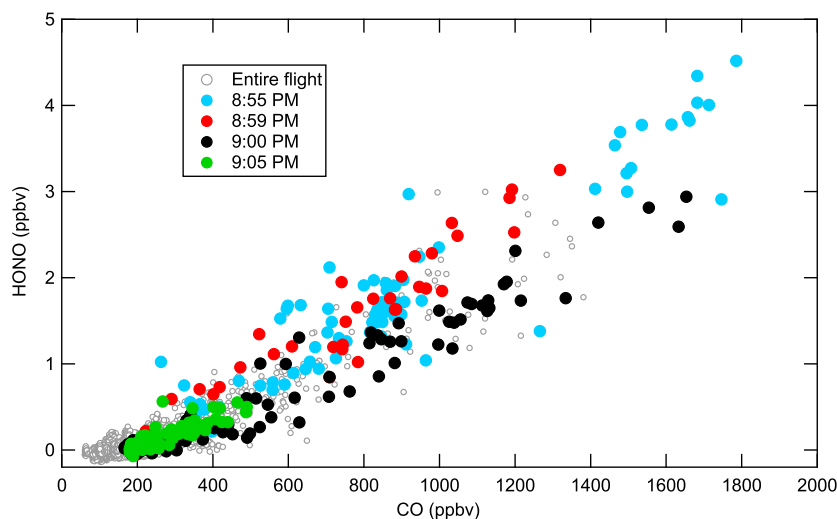


Figure 2. The 1 s measurements of HONO versus CO measured at night. The gray circles are all measurements from the flight that was conducted from 8 P.M. to 3 A.M. CDT on 2–3 July 2013. The colored circles were measured in the four spatially distinct fire plumes shown in Figure 1, with the time of each plume encounter shown in the legend.

HONO to NO_y enhancement ratio ($\text{HONO}:\text{NO}_y$, also determined using linear least squares fits of 1 s data in each plume) varied from 2 to 14% and was usually within the range of reported HONO to NO_x fire emission ratios measured from the air of 7.7–22% [Burling *et al.*, 2011].

HONO mixing ratios in some fire plumes were greater than the HONO detection limit of an onboard broadband cavity enhanced absorption spectrometer [Min *et al.*, 2016] used primarily for glyoxal and NO_2 detection. This instrument measured HONO with 9% accuracy and 350 pptv precision for 5 s data. In fire plumes where HONO exceeded 1 ppbv, the two HONO measurements agreed within their combined uncertainties (~50%), with the broadband cavity enhanced absorption spectrometer values about 25% larger than those reported by the CIMS. The agreement between independent instruments and with previous fire studies indicates that HONO was measured accurately.

3.2. Fire Plumes Sampled During Daytime

HONO was also measured in several fire plumes during the day, when the enhancement ratios of directly emitted compounds other than HONO were similar to those measured at night. But photolysis reduced HONO mixing ratios, resulting in substantially lower $\text{HONO}:\text{CO}$. For example, a fire plume measured during the day on 25 June 2013 had CO mixing ratios over 500 ppbv and a NO_y to CO enhancement ratio of 1%, similar to the fire plumes observed at night. In the daytime fire plumes, $\text{HONO}:\text{CO}$ was approximately one tenth the ratio observed at night, consistent with HONO loss by photolysis. Since there were many of these small agricultural fires and their locations were not precisely known, plume age and HONO production and loss rates could not be determined reliably for these daytime plumes. However, the substantial decrease in HONO relative to CO during the day demonstrates qualitatively that HONO photolysis was far faster than any potential HONO formation in fire plumes. The contrast between day and night measurements of HONO in fire plumes illustrates the value of quantifying HONO emissions ratios at night, when HONO is not photolyzed and emissions ratios are preserved over longer times.

3.3. Power Plant Plumes Sampled at Night

During SENEX, the aircraft sampled emissions from many electricity-generating power plants throughout the Southeast U.S. [Warneke *et al.*, 2016]. Emissions from these facilities provide an opportunity to examine HONO emissions and formation from large and well-characterized NO_x sources. At night, significant HONO enhancements were observed in some power plant plumes. Figure 3 shows measurements from two night flights conducted between 8 P.M. and 3 A.M. CDT on 1–3 July 2013, with measurements in plumes from the New Madrid, White Bluff, and Gaston power plants highlighted. These power plants burn coal as their primary fuel, generate 1.2–1.9 GW of electricity, and have stack heights between 230 and 305 m. Multiple crosswind plume transects were performed at altitudes ranging from 0.5 to 1.2 km agl. Nighttime winds varied considerably with altitude and ranged from 2 to 10 m s^{-1} during the plume measurements shown here. Multiple transects of the plume from the New Madrid power plant, located in southeast Missouri, were performed 20–50 km downwind from 9 to 11 P.M. CDT on 2 July 2013. Emissions from the White Bluff power plant, located in central Arkansas, were sampled 26–115 km downwind later in the evening on the same flight, between 12:30 and 1:37 A.M. CDT on 3 July 2013. $\text{HONO}:\text{NO}_y$ was 0.23% in the White Bluff and 0.18% in the New Madrid plumes (Figure 3). When NO_y was greater than 20 ppbv in the plumes, NO_y was predominately NO_x ($\text{NO}_x/\text{NO}_y > 85\%$), and HONO to NO_x enhancement ratios ($\text{HONO}:\text{NO}_x$) were similar to $\text{HONO}:\text{NO}_y$. In the concentrated plumes, the partitioning of NO_x between NO and NO_2 varied, and HONO was better correlated with NO_x than with either NO or NO_2 . The plume from the Gaston power plant in central Alabama was sampled on many flights, and the measurements from 10 P.M. to midnight CDT on 1–2 July 2013 are shown in Figure 3. Compared to the New Madrid and White Bluff power plants, HONO emissions from Gaston were a factor of 3–4 lower, with $\text{HONO}:\text{NO}_y = 0.06\%$. Several other power plants did not emit detectable HONO concentrations.

A summary of $\text{HONO}:\text{NO}_y$ measured in 20 transects of plumes from five different power plants on three night flights is shown in Figure 4. Only concentrated plumes with CO_2 and NO_y enhancements at least five times the background variability were included in the analysis (CO_2 enhancements greater than 5 ppmv and NO_y enhancements greater than 4 ppbv), and the source of each power plant plume was clearly identified using wind direction and location. $\text{HONO}:\text{NO}_y$ measured at night ranged from 0 to 0.4% and did not correlate with NO_x partitioning or transport time. The lack of dependence on plume age indicates that HONO was directly

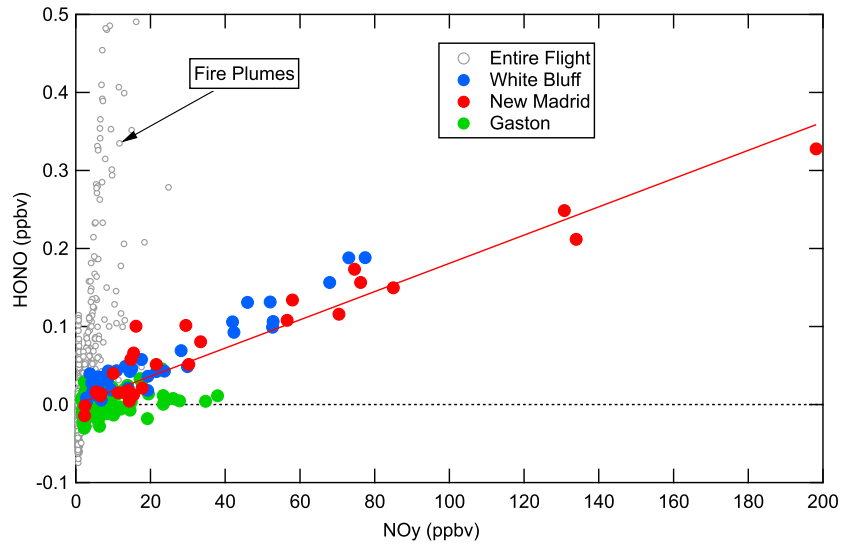


Figure 3. Measurements of HONO versus NO_y , averaged for 10 s. The gray circles were measured during the entire night flight over Arkansas and Tennessee shown in Figure 2. The HONO axis is expanded compared to Figure 2 to highlight the lower mixing ratios in power plant plumes, and many of the fire plume values are off scale. The red circles were measured in plumes from the New Madrid power plant, and the blue circles in plumes from the White Bluff power plant on 2–3 July 2013. The green circles were measured between 10 P.M. CDT and midnight on 1–2 July 2013 in plumes from the Gaston power plant. The red line is a linear least squares fit to the New Madrid plume measurements and has a slope of 0.18%. The dashed line is the ordinate zero.

emitted and not formed or lost during plume transport at night. This finding is consistent with previous work that has demonstrated that small NO_2 uptake coefficients [Kurtenbach *et al.*, 2001] results in negligible HONO production from heterogeneous reactions of NO_2 on aerosol [Stemmler *et al.*, 2007; VandenBoer *et al.*, 2013]. Further, nighttime observations with varying NO_x partitioning demonstrate that HONO enhancements in power plant plumes were from direct emissions.

3.4. Power Plant Plumes Sampled During Daytime

HONO enhancements in power plant plumes were also observed during the day, with HONO and NO_x strongly correlated. Figure 5 shows measurements during a daytime flight over and downwind of Atlanta, Georgia, where the largest HONO enhancements were in plumes from coal-burning electricity-generating

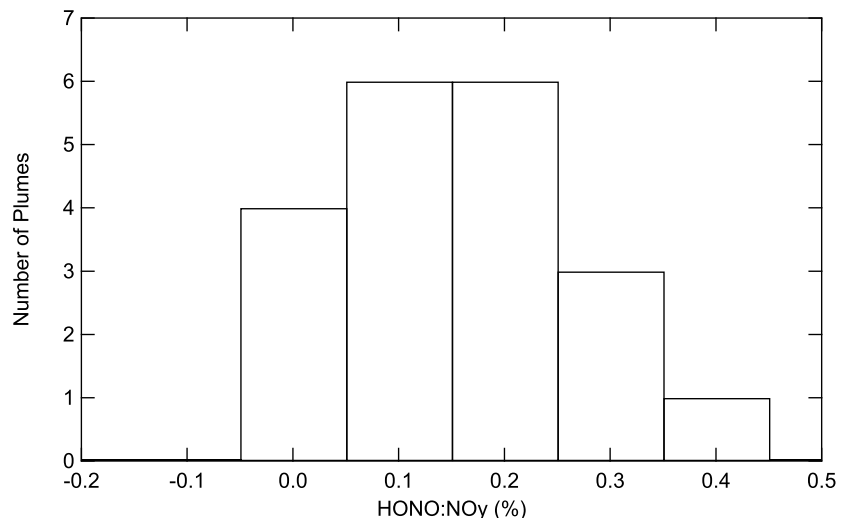


Figure 4. HONO: NO_y in 20 distinct power plant plumes measured at night.

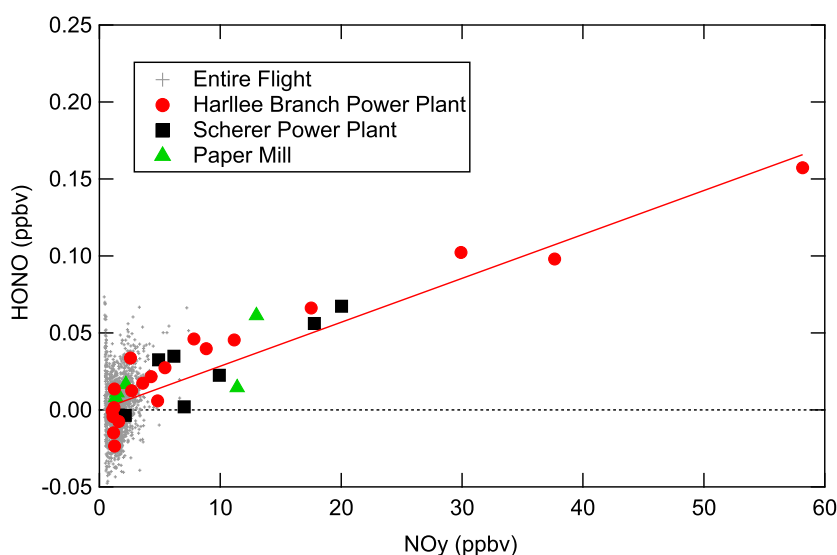


Figure 5. The 10 s averages of HONO versus NO_y on 16 June 2013 during a daytime flight in the vicinity of Atlanta, Georgia. The red circles were measured in two crosswind plume transects located 8 and 23 km downwind from the Harlee Branch power plant. The black squares were measured in a plume transect 22 km downwind from the Scherer power plant. The green triangles were measured downwind from a paper mill. The red line is a linear least squares fit to measurements in the Harlee Branch power plant plume and has a slope of 0.25%.

power plants. Measurements in the closest two crosswind transects of the Harlee Branch power plant plume and the closest transect of the Scherer power plant plume are highlighted in Figure 5. The 1.54 GW Harlee Branch plant and the 3.52 GW Scherer plant, which was the sixth largest power plant in the U.S. in 2012 by net power generation, exhaust gas through 300 m stacks. $\text{HONO}:\text{NO}_y$ was 0.25% in these plumes that were sampled 0.5–1 h after emission (Figure 5). Plume dilution rapidly reduced the atmospheric concentration of emitted compounds, rendering a detailed analysis of HONO production and loss rates unfeasible. For example, NO_x and SO_2 enhancements in the Harlee Branch power plant plume were diluted by a factor of 8 between the first transect 8 km downwind and the next transect 23 km downwind. Rapid dilution and loss reduced HONO to levels near its detection limit so that HONO photochemistry as a function of time since emission could not be studied reliably for a single plume. Since these plumes were sampled downwind after transport over several HONO photolysis lifetimes, the daytime measurements are not used to assess direct HONO emissions.

3.5. Urban and Rural Regions Sampled at Night

Several flights sampled atmospheric emissions and subsequent processing from urban areas, including Atlanta, Birmingham, Indianapolis, and St. Louis. The aircraft sampled the PBL upwind and over these urban areas and performed multiple crosswind transects of urban plumes at different distances downwind. Urban plumes were measured both day and night, and plumes from Atlanta and Birmingham were sampled on multiple flights. The nighttime Atlanta urban plume was sampled at 10:45 P.M. EDT (local time), on 19 June, when sunset in Atlanta was 8:51 P.M. EDT. The plume was intercepted 60 km WSW of Atlanta at 0.6 km agl, where winds were from the direction of Atlanta (ENE at 8.5 m s^{-1}). Enhancement ratios of several compounds were indicative of the Atlanta urban source. The CO to NO_y enhancement ratio was approximately 4, consistent with an urban source dominated by vehicle emissions [Parrish, 2006]. Fire and power plant sources can be ruled out based upon the enhancement ratios of CO and SO_2 to NO_y . Figure 6 shows 10 s average measurements of HONO and NO_y for the entire flight conducted from 6:30 P.M. to 12:30 A.M. EDT on 19–20 June 2013. In the Atlanta plume, shown as red circles in Figure 6, HONO reached 200 pptv and was correlated with NO_y with a slope of 0.9%. The ratio is slightly larger than $\text{HONO}:\text{NO}_x = 0.3\text{--}0.8\%$ reported for direct emissions from vehicles [Kirchstetter et al., 1996; Kurtenbach et al., 2001; Stutz et al., 2002]. For most of the rest of this night flight near Atlanta, NO_y was <5 ppbv and 10 s HONO averaged -2 ± 17 pptv. Figure 6 also includes measurements in plumes from coal-fired power plants near Atlanta, where HONO enhancements were small.

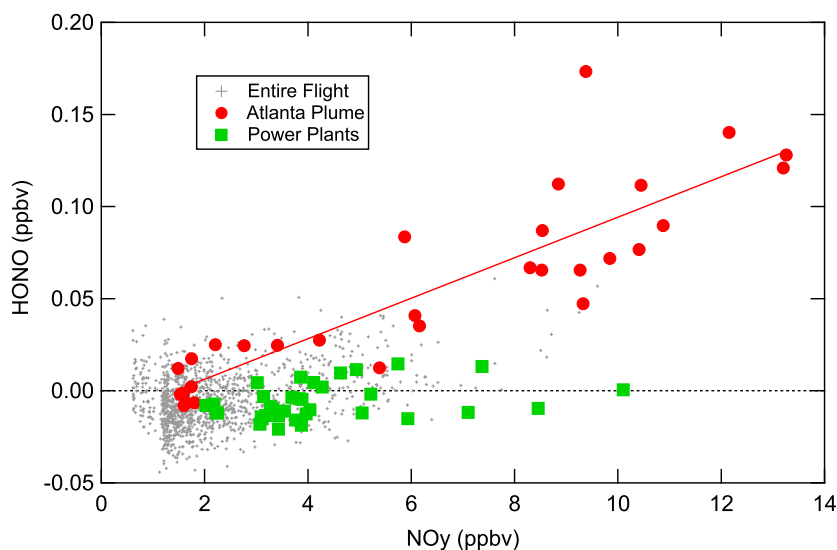


Figure 6. The 10 s averages of HONO versus NO_y measured at night on 19 June 2013 (gray circles). The red circles were measured in a plume transported 60 km from Atlanta, Georgia, and the green squares were measured in plumes from coal-fired power plants.

3.6. Urban and Rural Regions Sampled During Daytime

In urban plumes, mixing ratios of HONO and other reactive nitrogen species were small compared to plumes from point sources. The flight on 16 June 2013, which was conducted between 11:16 A.M. and 5:48 P.M. EDT upwind and downwind of Atlanta, and also sampled emissions from several power plants in Georgia, represents typical conditions encountered in these daytime urban plume studies. Measurements of HONO and NO_y for this entire daytime flight are shown in Figure 5, using 10 s averages of the 1 s data. Most of the flight was conducted between 0.4 and 0.7 km agl, with three vertical profiles to 3 km altitude and 20 min transits between Tennessee and Georgia conducted between 3 and 5 km altitude. In the PBL over Atlanta and up to 50 km downwind, NO_x was ~ 3 ppbv, with higher concentrations in spatially compact plumes sampled within several kilometers downwind from power plants. Upwind of Atlanta and in Atlanta plume transects more than 50 km downwind, NO_x was 0.2–0.5 ppbv. HONO averaged 2 ± 18 pptv for 10 s averages (gray circles in Figure 5) for the entire flight, exclusive of the plumes from point sources highlighted in Figure 5. Similarly, HONO mixing ratios were below the detection limit in the PBL during other daytime flights in the vicinity of urban areas. Over rural areas, reactive nitrogen mixing ratios were even smaller, and HONO remained below the detection limit. For example, reactive nitrogen mixing ratios in the PBL upwind of Atlanta and outside of the power plant plumes shown in Figure 5 were low, with $\text{NO} = 23 \pm 12$ pptv, $\text{NO}_2 = 190 \pm 68$ pptv, $\text{HNO}_3 = 296 \pm 41$ pptv, and $\text{HONO} = -4 \pm 11$ pptv, where the mixing ratios are the averages during a 12 min period and the standard deviation about the means are determined for 10 s averaged data.

HONO mixing ratios were greater than background values in plumes from other industrial facilities sampled during both day and night, including paper mills and cement plants, with HONO: NO_y that ranged from 0.1 to 0.4%. For example, the green triangles in Figure 5 are from measurements downwind from a paper mill located in Macon, Georgia, where HONO: NO_y was similar to that in the power plant plumes. In plumes from industrial facilities that were not large NO_x emitters, HONO increases were not observed. For example, over 100 ppbv enhancements in CO mixing ratios were observed in plumes from a steel plant near Birmingham, Alabama. NO_y enhancements were only 3 ppbv, and HONO remained below the detection limit.

4. Discussion

4.1. Direct HONO Emissions

HONO was enhanced in many plumes from power plants and agricultural fires. HONO emission factors from fires have been studied in laboratories and the atmosphere, and the results measured here at several

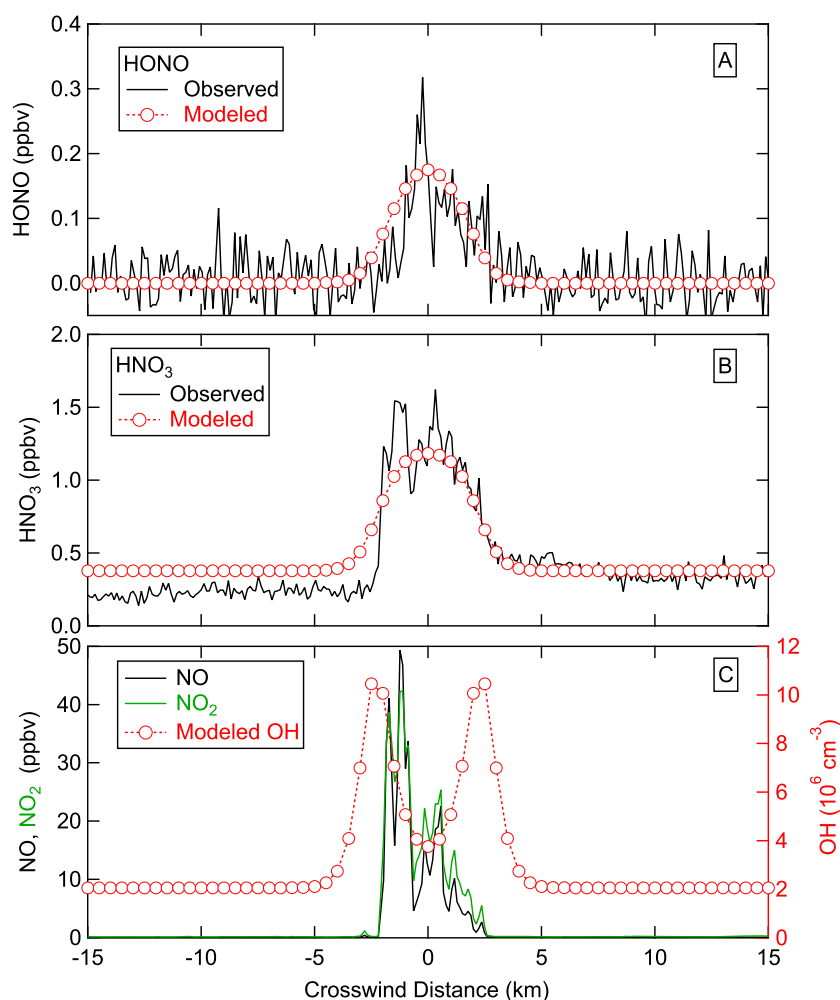


Figure 7. (a) Measured and modeled daytime HONO 8 km downwind from the Harlee Branch power plant at 0.6 km agl on 16 June 2013. (b) The same as Figure 7a but for HNO₃. (c) The 1 s measurements of NO (black), NO₂ (green), and modeled OH in the same plume.

hundred meters above ground level in the PBL are similar to those findings. The high nitrogen content of biomass and the possibility of secondary formation of HONO on aerosols in fire plumes [Veres *et al.*, 2010b] resulted in HONO:NO_y emitted from flaming combustion that ranged from 2 to 14% and was larger than HONO:NO_y emitted from fossil fuel combustion. Direct emission of HONO was observed from some power plants, with emitted HONO:NO_y that ranged from 0 to 0.4% and was much lower than fire emissions. The emitted HONO:NO_y from power plants were less than or similar to other fossil fuel combustion sources, including aircraft (HONO:NO_y = 0.5–7% [Wood *et al.*, 2008; Lee *et al.*, 2011; Jurkat *et al.*, 2011]) and motor vehicles (HONO:NO_x = 0.3–0.8% [Kirchstetter *et al.*, 1996; Kurtenbach *et al.*, 2001]). We do not know why HONO emissions from power plants were variable and often less than from other combustion sources.

4.2. Daytime HONO Formation in Power Plant Plumes

HONO production and loss processes are examined by comparing the daytime measurements in power plant plumes with a Lagrangian plume dispersion model [Sillman, 2000; Wert *et al.*, 2003]. For example, Figure 7 shows 1 s measurements and model results for the closest plume transect from the Harlee Branch power plant, described in section 3.4. The wind speed was 4 m s⁻¹, and the plume was sampled about 0.5 h after emission. More than 200 pptv HONO was formed at the plume center, ozone was titrated from 45 ppbv to 10 ppbv, and 1.3 ppbv of HNO₃ was produced. The observed HONO:NO_y in the plume illustrated in Figure 7 was 0.2%. For the plume modeling, hourly NO_x emissions were obtained from continuous emissions monitoring systems in the plant stacks. Direct HONO emissions were not included, since the plumes were

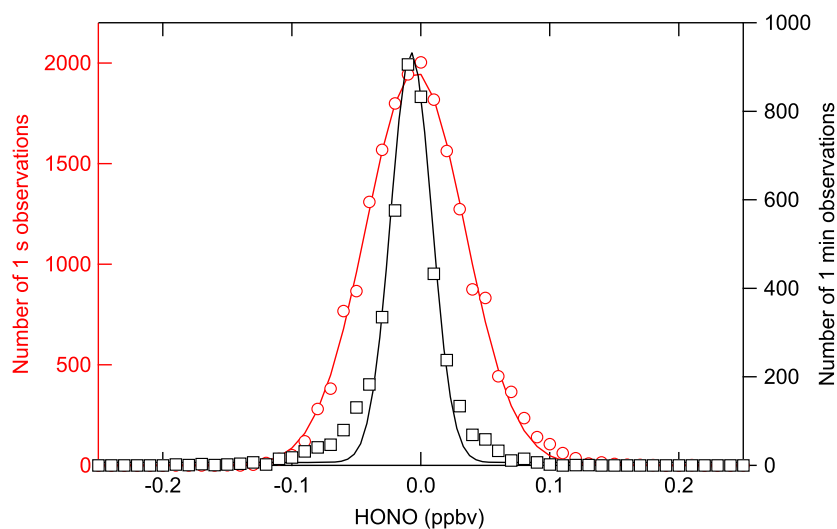


Figure 9. Frequency distribution of 1 s HONO observations on 16 June 2013 over Georgia and Tennessee from 11:16 A.M. to 5:49 P.M. EDT, shown for 10 pptv HONO intervals (red symbols). The black symbols are the frequency distribution for 1 min HONO averages from 14 daytime flights. The measurements have been fit with normal distributions with widths of 38 pptv (red line) and 16 pptv (black line).

Figure 9. The observations are fit with a normal distribution of the functional form $e^{-\frac{(x-x_0)^2}{2\sigma^2}}$, centered about $x_0 = -4$ pptv HONO and with a width $\sigma = 38$ pptv. The width of this distribution is consistent with the 40 pptv measurement uncertainty for 1 s data, determined from a 25 pptv measurement imprecision and a 30 pptv uncertainty from instrument background variability. Averaging the 1 s data reduces HONO measurement uncertainty. The frequency distribution for 1 min HONO averages from 14 daytime flights is fit by a normal distribution with a 16 pptv width (Figure 9). The median HONO mixing ratio for each of the 14 daytime flights ranged from -15 pptv to 10 pptv. This spread in median values was caused by background variability and inaccuracy that imposes a 15 pptv uncertainty on the HONO measurements and limits the effectiveness of averaging.

The average daytime HONO mixing ratios observed here are consistent with the levels expected from gas phase production and an 11 min photolysis lifetime [Stockwell and Calvert, 1978] during these summer mid-day measurements. Outside of concentrated plumes very close (tens of kilometers) to strong NO_x emission sources, PSS calculation gives $\text{HONO} \cong 1$ pptv during these summer daytime flights. These measurements show that a widespread unknown source or other in situ HONO sources, such as the reaction of NO_2 on humid surfaces [Stutz *et al.*, 2004], did not increase HONO to levels greater than approximately 15 pptv throughout the PBL.

4.4. Atmospheric Implications

Daytime HONO mixing ratios measured outside of fresh combustion plumes were smaller than in many previous reports. Differences may be attributed partially to the time and altitude of these aircraft measurements that do not necessarily reveal ground-level HONO mixing ratios. Even in a well-mixed boundary layer, HONO mixing ratios may change dramatically with height above the ground [Young *et al.*, 2012], since HONO photolysis lifetimes can be less than boundary layer mixing times. The largest HONO mixing ratios typically have been observed at ground level in polluted urban areas at night, and many studies have shown decreasing HONO mixing ratios with altitude in the lowest few hundred meters of the troposphere [Kleffmann, 2007; Young *et al.*, 2012; VandenBoer *et al.*, 2013]. Most daytime sampling here was performed between 0.5 and 0.6 km agl and within the PBL, and the aircraft descended below 0.4 km agl on only a few occasions. The aircraft did not sample air masses where the largest HONO mixing ratios have been observed, since no flights were conducted within several hours of sunrise and the aircraft usually stayed several hundred meters above the ground. Although differing sampling environments may account for some disparity between these results and previous reports, the daytime HONO mixing ratios reported here are much less than the

tens to hundreds of pptv that have been reported several hundred meters above ground level from other daytime tropospheric measurements [Zhang *et al.*, 2009; Häselser *et al.*, 2009; Zhou *et al.*, 2011; Wong *et al.*, 2012; Li *et al.*, 2014].

After sunset, HONO photolysis ceases, and conversion of NO₂ to HONO at the surface can cause HONO to build up at night to reach a maximum in the evening or just before sunrise. In the Atlanta plume measured from the WP-3D aircraft at night, HONO:NO_y was 0.9% and similar to reported emission ratios from cars. This lack of substantial nighttime HONO buildup measured from the aircraft may be a consequence of sampling in residual layers that were decoupled from ground-level sources of HONO, such as conversion of NO₂ to HONO on surfaces in shallow confined layers. Consequently, urban plumes sampled at night in the residual layer may not experience a HONO buildup as they do at the surface.

In plumes from urban and industrial combustion sources measured from aircraft, HONO enhancements were explained entirely by direct emissions and gas phase photochemical formation. The HONO formation in power plant plumes reported here is an internal source of HONO that consumes OH and NO and does not alter HO_x or NO_x budgets. Outside of these plumes, HONO mixing ratios were below the detection limit and indistinguishable from zero. Known HONO sources adequately account for all of these observations, and no evidence was found for unknown sources. These findings that examine HONO distributions above ground level further support work that showed ground-based HONO measurements overestimated the impact of HONO on radical budgets for the entire boundary layer [Young *et al.*, 2012].

Acknowledgments

We thank the NOAA WP-3D flight and support crew for the many successful flights. Data can be accessed from esrl.noaa.gov/csd/projects/senex/.

References

- Akagi, S. K., R. J. Yokelson, C. Wiedinmyer, M. J. Alvarado, J. S. Reid, T. Karl, J. D. Crouse, and P. O. Wennberg (2011), Emission factors for open and domestic biomass burning for use in atmospheric models, *Atmos. Chem. Phys.*, *11*, 4039–4072, doi:10.5194/acp-11-4039-2011.
- Baergen, A. M., S. A. Styler, D. van Pinxteren, K. Müller, H. Herrmann, and D. J. Donaldson (2015), Chemistry of urban grime: Inorganic ion composition of grime vs particles in Leipzig, Germany, *Environ. Sci. Technol.*, *49*, 12,688–12,696, doi:10.1021/acs.est.5b03054.
- Burling, I. R., R. J. Yokelson, S. K. Akagi, S. P. Urbanski, C. E. Wold, D. W. T. Griffith, T. J. Johnson, J. Reardon, and D. R. Weise (2011), Airborne and ground-based measurements of the trace gases and particles emitted by prescribed fires in the United States, *Atmos. Chem. Phys.*, *11*, 12,197–12,216, doi:10.5194/acp-11-12197-2011.
- Calvert, J. G., G. Yarwood, and A. M. Dunker (1994), An evaluation of the mechanism of nitrous acid formation in the urban atmosphere, *Res. Chem. Intermed.*, *20*, 463–502.
- Czader, B. H., B. Rappenglück, P. Percell, D. W. Byun, F. Ngan, and S. Kim (2012), Modeling nitrous acid and its impact on ozone and hydroxyl radical during the Texas Air Quality Study 2006, *Atmos. Chem. Phys.*, *12*, 6939–6951, doi:10.5194/acp-12-6939-2012.
- Gall, E. T., et al. (2016), Evaluation of nitrous acid sources and sinks in urban outflow, *Atmos. Environ.*, *127*, 272–282.
- Häselser, R., T. Brauers, F. Holland, and A. Wahner (2009), Development and application of a new mobile LOPAP instrument for the measurement of HONO altitude profiles in the planetary boundary layer, *Atmos. Meas. Tech. Discuss.*, *2*, 2027–2054.
- Holloway, J. S., R. O. Jakoubek, D. D. Parrish, C. Gerbig, A. Volz-Thomas, S. Schmitgen, A. Fried, B. Wert, B. Henry, and J. R. Drummond (2000), Airborne intercomparison of vacuum ultraviolet fluorescence and tunable diode laser absorption measurements of tropospheric carbon monoxide, *J. Geophys. Res.*, *105*, 24,251–24,261, doi:10.1029/2000JD900237.
- Jurkat, T., C. Voigt, F. Arnold, H. Schlager, J. Kleffmann, H. Aufmhoff, D. Schäuble, M. Schaefer, and U. Schumann (2011), Measurements of HONO, NO, NO_y and SO₂ in aircraft exhaust plumes at cruise, *Geophys. Res. Lett.*, *38*, L10807, doi:10.1029/2011GL046884.
- Kirchstetter, T. W., R. A. Harley, and D. Littlejohn (1996), Measurement of nitrous acid in motor vehicle exhaust, *Environ. Sci. Technol.*, *30*, 2843–2849.
- Kleffmann, J. (2007), Daytime sources of nitrous acid (HONO) in the atmospheric boundary layer, *Chem. Phys. Chem.*, *8*, 1137–1144, doi:10.1002/cphc.200700016.
- Kleffmann, J., and P. Wiesen (2008), Technical note: Quantification of interferences of wet chemical HONO LOPAP measurements under simulated polar conditions, *Atmos. Chem. Phys.*, *8*, 6813–6822.
- Kleffmann, J., R. Kurtenbach, J. Lörzer, P. Wiesen, N. Kalthoff, B. Vogel, and H. Vogel (2003), Measured and simulated vertical profiles of nitrous acid. Part I: Field measurements, *Atmos. Environ.*, *37*, 2949–2955.
- Kurtenbach, R., K. H. Becker, J. A. G. Gomes, J. Kleffmann, J. C. Lörzer, M. Spittler, P. Wiesen, R. Ackermann, A. Geyer, and U. Platt (2001), Investigations of emissions and heterogeneous formation of HONO in a road traffic tunnel, *Atmos. Environ.*, *35*, 3385–3394.
- Lammel, G., and J. N. Cape (1996), Nitrous acid and nitrite in the atmosphere, *Chem. Soc. Rev.*, *25*, 361–369.
- Lee, B. H., G. W. Santoni, E. C. Wood, S. C. Herndon, R. C. Miake-Lye, M. S. Zahniser, S. C. Wofsy, and J. W. Munger (2011), Measurements of nitrous acid in commercial aircraft exhaust at the alternative aviation fuel experiment, *Environ. Sci. Technol.*, *45*, 7648–7654, doi:10.1021/es200921t.
- Lee, B. H., E. C. Wood, S. C. Herndon, B. L. Lefer, W. T. Luke, W. H. Brune, D. D. Nelson, M. S. Zahniser, and J. W. Munger (2013), Urban measurements of atmospheric nitrous acid: A caveat on the interpretation of the HONO photostationary state, *J. Geophys. Res. Atmos.*, *118*, 12,274–12,281, doi:10.1002/2013JD020341.
- Lee, B. H., F. D. Lopez-Hilfiker, C. Mohr, T. Kurtén, D. R. Worsnop, and J. A. Thornton (2014), An iodide-adduct high-resolution time-of-flight chemical-ionization mass spectrometer: Application to atmospheric inorganic and organic compounds, *Environ. Sci. Technol.*, *48*, 6309–6317, doi:10.1021/es500362a.
- Li, X., et al. (2014), Missing gas-phase source of HONO inferred from Zeppelin measurements in the troposphere, *Science*, *344*, 292–296, doi:10.1126/science.1248999.
- Min, K.-E., et al. (2016), A broadband cavity enhanced absorption spectrometer for aircraft measurements of glyoxal, methylglyoxal, nitrous acid, nitrogen dioxide, and water vapor, *Atmos. Meas. Tech.*, *9*, 423–440, doi:10.5194/amt-9-423-2016.

- Müller, M., et al. (2016), In situ measurements and modeling of reactive trace gases in a small biomass burning plume, *Atmos. Chem. Phys.*, *16*, 3813–3824, doi:10.5194/acp-16-3813-2016.
- Neuman, J. A., et al. (2002), Fast-response airborne in situ measurements of HNO₃ during the Texas air quality study, *J. Geophys. Res.*, *107*(D20), 4436, doi:10.1029/2001JD001437.
- Neuman, J. A., T. B. Ryerson, L. G. Huey, R. Jakoubek, J. B. Nowak, C. Simons, and F. C. Fehsenfeld (2003), Calibration and evaluation of nitric acid and ammonia permeation tubes by UV optical absorption, *Environ. Sci. Technol.*, *37*, 1975–1981, doi:10.1021/ES06422L.
- Neuman, J. A., et al. (2010), Bromine measurements in ozone depleted air over the Arctic Ocean, *Atmos. Chem. Phys.*, *10*, 6503–6514, doi:10.5194/acp-10-6503-2010.
- Oswald, R., et al. (2013), HONO Emissions from soil bacteria as a major source of atmospheric reactive nitrogen, *Science*, *341*, 1233–1235, doi:10.1126/science.1242266.
- Parrish, D. D. (2006), Critical evaluation of US on-road vehicle emission inventories, *Atmos. Environ.*, *40*, 2288–2300, doi:10.1016/j.atmosenv.2005.11.033.
- Perner, D., and U. Platt (1979), Detection of nitrous acid in the atmosphere by differential optical absorption spectroscopy, *Geophys. Res. Lett.*, *6*(2), 917–920, doi:10.1029/GL006i012p00917.
- Pollack, I. B., B. M. Lerner, and T. B. Ryerson (2011), Evaluation of ultraviolet light-emitting diodes for detection of atmospheric NO₂ by photolysis-chemiluminescence, *J. Atmos. Chem.*, doi:10.1007/s10874-01109184-3.
- Roberts, J. M., et al. (2010), Measurement of HONO, HNCO, and other inorganic acids by negative-ion proton-transfer chemical-ionization mass spectrometry (NI-PT-CIMS): Application to biomass burning emissions, *Atmos. Meas. Tech.*, *3*, 981–990, doi:10.5194/amt-3-981-2010.
- Sander, S. P., et al. (2006), Chemical kinetics and photochemical data for use in atmospheric studies, evaluation number 15, JPL Publ., 06-2, Pasadena, Calif.
- Sillman, S. (2000), Ozone production potential and loss of NO_x in power plant plumes: Photochemical model and interpretation of measurements in Tennessee, *J. Geophys. Res.*, *105*, 9189–9202, doi:10.1029/1999JD901014.
- Stemmler, K., M. Ammann, C. Donders, J. Kleffmann, and C. George (2006), Photosensitized reduction of nitrogen dioxide on humic acid as a source of nitrous acid, *Nature*, *440*, doi:10.1038/nature04603.
- Stemmler, K., M. Ndour, Y. Elshorbany, J. Kleffmann, B. D'Anna, C. George, B. Bohn, and M. Ammann (2007), Light induced conversion of nitrogen dioxide into nitrous acid on submicron humic acid aerosol, *Atmos. Chem. Phys.*, *7*, 4237–4248.
- Stockwell, W. R., and J. G. Calvert (1978), The near ultraviolet absorption spectrum of gaseous HONO and N₂O₃, *J. Photochem.*, *8*, 193–203.
- Stutz, J., B. Alicke, and A. Neftel (2002), Nitrous acid formation in the urban atmosphere: Gradient measurements of NO₂ and HONO over grass in Milan, Italy, *J. Geophys. Res.*, *107*(D22), 8192, doi:10.1029/2001JD000390.
- Stutz, J., B. Alicke, R. Ackermann, A. Geyer, S. Wang, A. B. White, E. J. Williams, C. W. Spicer, and J. D. Fast (2004), Relative humidity dependence of HONO chemistry in urban areas, *J. Geophys. Res.*, *109*, D03307, doi:10.1029/2003JD004135.
- VandenBoer, T. C., et al. (2013), Understanding the role of the ground surface in HONO vertical structure: High resolution vertical profiles during NACHTT-11, *J. Geophys. Res. Atmos.*, *118*, 10,155–10,171, doi:10.1002/jgrd.50721.
- VandenBoer, T. C., C. J. Young, R. K. Talukdar, M. Z. Markovic, S. S. Brown, J. M. Roberts, and J. G. Murphy (2015), Nocturnal loss and daytime source of nitrous acid through reactive uptake and displacement, *Nat. Geosci.*, *8*, 55–60, doi:10.1038/ngeo2298.
- Veres, P., J. B. Gilman, J. M. Roberts, W. C. Kuster, C. Warneke, I. R. Burling, and J. de Gouw (2010a), Development and validation of a portable gas phase standard generation and calibration system for volatile organic compounds, *Atmos. Meas. Tech.*, *3*, 683–691, doi:10.5194/amt-3-683-2010.
- Veres, P., J. M. Roberts, I. R. Burling, C. Warneke, J. de Gouw, and R. J. Yokelson (2010b), Measurements of gas phase inorganic and organic acids from biomass fires by negative-ion proton-transfer chemical-ionization mass spectrometry, *J. Geophys. Res.*, *115*, D23302, doi:10.1029/2010JD014033.
- Warneke, C., et al. (2016), Instrumentation and measurement strategy for the NOAA SENEX aircraft campaign as part of the Southeast Atmosphere Study 2013, *Atmos. Meas. Tech.*, doi:10.5194/amt-2015-388.
- Wert, B. P., et al. (2003), Signatures of terminal alkene oxidation in airborne formaldehyde measurements during TexAQS 2000, *J. Geophys. Res.*, *108*(D3), 4104, doi:10.1029/2002JD002502.
- Wong, K. W., C. Tsai, B. Lefer, C. Haman, N. Grossberg, W. H. Brune, X. Ren, W. Luke, and J. Stutz (2012), Daytime HONO vertical gradients during SHARP 2009 in Houston, TX, *Atmos. Chem. Phys.*, *12*, 635–652, doi:10.5194/acp-12-635-2012.
- Wood, E. C., S. C. Herndon, M. T. Timko, P. E. Yelvington, and R. C. Miake-Lye (2008), Speciation and chemical evolution of nitrogen oxides in aircraft exhaust near airports, *Environ. Sci. Technol.*, *42*, 1884–1891, doi:10.1021/es072050a.
- Yokelson, R. J., T. Karl, P. Artaxo, D. R. Blake, T. J. Christian, D. W. T. Griffith, A. Guenther, and W. M. Hao (2007), The Tropical Forest and Fire Emissions Experiment: Overview and airborne fire emission factor measurements, *Atmos. Chem. Phys.*, *7*, 5175–5196.
- Young, C. J., et al. (2012), Vertically resolved measurements of nighttime radical reservoirs in Los Angeles and their contribution to the urban radical budget, *Environ. Sci. Technol.*, *46*, 10,965–10,973, doi:10.1021/es302206a.
- Zhang, N., X. Zhou, P. B. Shepson, H. Gao, M. Alaghmand, and B. Stirm (2009), Aircraft measurement of HONO vertical profiles over a forested region, *Geophys. Res. Lett.*, *36*, L15820, doi:10.1029/2009GL038999.
- Zhou, X., et al. (2011), Nitric acid photolysis on forest canopy surface as a source for tropospheric nitrous acid, *Nat. Geosci.*, *4*, 440–443.